Journal of Biomedical Research

SBMB-004: A first-in-class dual MDM2/BRD4 inhibitor restoring p53 function and suppressing oncogenic transcription in acute myeloid leukemia

Mohammad Abohassan, Mesfer Mohammad Al Shahrani, Prasanna Rajagopalan

Cite this article as:
Mohammad Abohassan, Mesfer Mohammad Al Shahrani, Prasanna Rajagopalan. SBMB–004: A first–in–class dual MDM2/BRD4 inhibitor restoring p53 function and suppressing oncogenic transcription in acute myeloid leukemia[J]. *Journal of Biomedical Research*, In press. doi: 10.7555/JBR.39.20250492

View online: https://doi.org/10.7555/JBR.39.20250492

Available online at www.jbr-pub.org.cn

Open Access at PubMed Central

Journal of Biomedical Research, 2026 40(0): 1–18

Original Article

JBR

SBMB-004: A first-in-class dual MDM2/BRD4 inhibitor restoring p53 function and suppressing oncogenic transcription in acute myeloid leukemia

Mohammad Abohassan[1,2], Mesfer Mohammad Al Shahrani[1], Prasanna Rajagopalan[1,✉]

[1]*Department of Clinical Laboratory Sciences, College of Applied Medical Sciences, King Khalid University, Abha, Saudi Arabia;*
[2]*Health and Medical Research Centre, King Khalid University, Abha 61421, Saudi Arabia.*

Abstract

Acute myeloid leukemia (AML) remains difficult to treat due to relapse and therapeutic resistance driven by convergent oncogenic pathways. Overexpression of murine double minute 2 (MDM2) suppresses the tumor suppressor activity of p53, while bromodomain-containing protein 4 (BRD4) sustains oncogenic transcriptional programs; together, these mechanisms promote leukemic survival. Given the limited durability of single-pathway inhibition, we employed a structure-guided virtual screening approach using the ChemBridge library to identify dual modulators targeting the MDM2 pocket and BRD4 bromodomains. The lead compound, SBMB-004, was characterized through molecular docking, 100-ns molecular dynamics simulations, and Molecular Mechanics Poisson–Boltzmann Surface Area (MM/PBSA) binding free energy analyses, followed by biochemical and cellular validation. SBMB-004 demonstrated potent dual inhibition of MDM2 (half maximal inhibitory concentration [IC_{50}] = 80.08 nmol/L) and BRD4 (IC_{50} = 95.15 nmol/L) in time-resolved fluorescence resonance energy transfer (TR-FRET) assays. In AML cell models, it exhibited selective anti-proliferative activity with 50% growth inhibition (GI_{50}) values of 110.9 nmol/L in THP-1 (p53-WT), 356.1 nmol/L in SKM-1 (mutant p53), and 1.75 μmol/L in U937 (p53-null) cells, while sparing normal HS-5 stromal cells (GI_{50} > 3.6 μmol/L). SBMB-004 induced time-dependent intracellular p53 stabilization in p53-competent cells and triggered apoptosis preferentially in wild-type contexts, with additional BRD4-mediated cytotoxic effects observed in p53-defective models. Collectively, these findings establish SBMB-004 as a first-in-class dual MDM2/BRD4 inhibitor and support multitargeted pathway modulation as a rational strategy to restore p53 signaling and counteract transcriptional resistance mechanisms in AML.

Keywords: acute myeloid leukemia, MDM2/BRD4/dual inhibitor, p53 stabilization, oncogenic transcription, apoptosis, small-molecule therapeutics

Introduction

Acute myeloid leukemia (AML) is one of the most aggressive and heterogeneous hematologic malignancies, characterized by the clonal expansion of immature myeloid progenitors in the bone marrow and peripheral blood[1]. Despite advances in diagnostic tools and therapeutic regimens, AML remains a major

✉Corresponding author: Prasanna Rajagopalan, E-mail: prachu.rg@gmail.com, ORCID: 0000-0001-7593-7234.

Received: 19 November 2025; Revised: 12 April 2026; Accepted: 18 April 2026;

CLC number: R733.71, R979.1, Document code: A

The authors reported no conflict of interests.

https://doi.org/10.7555/JBR.39.20250492

clinical challenge. Standard frontline treatments rely heavily on intensive chemotherapy, often in combination with stem cell transplantation for eligible patients. While these approaches can induce remission in many cases, relapse is frequent, and long-term survival rates remain dismal, particularly among older patients or those with therapy-resistant disease[2]. Recent studies have highlighted the genetic and molecular heterogeneity of AML, which contributes to variability in treatment responses and underscores the urgent need for novel therapeutic strategies capable of simultaneously targeting multiple oncogenic pathways[3].

One of the best-characterized tumor suppressor pathways in AML is the p53 regulatory axis. The transcription factor p53 plays a central role in maintaining genomic integrity by inducing cell cycle arrest, apoptosis, or senescence in response to DNA damage or oncogenic stress[4]. However, in AML, p53 activity of is frequently suppressed not by direct mutation but through the overexpression of its negative regulator, murine double minute 2 homolog (MDM2)[5]. MDM2 is an E3 ubiquitin ligase that binds to the transactivation domain of p53, leading to its ubiquitination and proteasomal degradation[6]. Elevated MDM2 levels diminish p53 activity, thereby allowing leukemic cells to evade apoptosis and proliferate unchecked[6]. Consequently, targeting the MDM2–p53 interaction has emerged as a promising therapeutic strategy, with several small-molecule inhibitors currently in clinical trials[7]. These inhibitors aim to restore p53 function and re-establish its tumor suppressive activity in AML cells[8]. However, challenges such as dose-limiting toxicities and the development of resistance highlight the need for combination or multitargeted strategies.

Alongside the disruption of the p53 pathway, aberrant transcriptional regulation is another hallmark of AML pathogenesis. Epigenetic modulators, particularly bromodomain-containing proteins, play a crucial role in maintaining leukemic transcriptional programs[9]. Bromodomain-containing protein 4 (BRD4), a member of the bromodomain and extra-terminal (BET) family, functions as an epigenetic reader that recognizes acetylated lysine residues on histone tails[10]. By binding to acetylated chromatin, BRD4 recruits transcriptional machinery, including the positive transcription elongation factor b (P-TEFb), thereby sustaining the expression of key oncogenes such as *MYC*[11]. Dysregulation of BRD4-driven transcription directly contributes to leukemogenesis by maintaining proliferation and blocking differentiation[12]. Small-molecule BET inhibitors have shown preclinical efficacy in AML by suppressing oncogenic transcription and promoting differentiation of leukemic blasts. However, similar to MDM2 inhibitors, BET inhibitors as single agents have demonstrated limited durability in clinical settings due to the emergence of adaptive resistance and compensatory signaling pathways[13].

Considering the complementary oncogenic roles of MDM2 and BRD4, a strategy that simultaneously targets both pathways holds significant therapeutic promise[14]. MDM2 inhibition can restore p53 function and trigger apoptosis, while BRD4 inhibition downregulates transcriptional programs critical for leukemic cell survival. The convergence of these effects may yield more robust and sustained anti-leukemic responses compared with modulating either pathway alone. Furthermore, dual targeting may help overcome resistance mechanisms arising from tumor plasticity and signaling redundancy[15]. Importantly, this strategy is consistent with the emerging paradigm in oncology that favors multitargeted approaches to address complex and heterogeneous disease networks, particularly in cancers such as AML where single-agent therapies often fail to achieve durable responses[16].

In this study, we employed a structure-guided, bioinformatics-driven discovery pipeline to identify and characterize SBMB-004 as a potential dual modulator of MDM2 and BRD4 in acute myeloid leukemia (AML). Instead of *de novo* medicinal chemistry design, SBMB-004 was prioritized through high-throughput virtual screening against the structurally defined binding sites of MDM2 and BRD4, followed by molecular docking, molecular dynamics simulations, and binding free energy calculations to evaluate its predicted binding affinity and engagement with both targets. The computational prioritization was subsequently complemented by biochemical and cellular validation in AML models to assess the functional relevance of concurrent MDM2 and BRD4 inhibition. By integrating structure-based screening with experimental validation, this work establishes a proof-of-concept framework for identifying multitarget small-molecule inhibitors for AML therapy.

Materials and methods

Structural retrieval and high-throughput virtual screening

The three-dimensional structure of the MDM2 protein was modeled using the SWISS-MODEL

Server (https://swissmodel.expasy.org), with PDB entry 4OGN as a template. The modeled structure was retrieved along with the reference ligand (AM-6761; 2U5), associated with 4OGN[17]. The structures of BRD4-BD1 and BRD4-BD2 were downloaded from the Protein Data Bank (PDB) with accession codes 3MXF and 4KV4, respectively. High-throughput virtual screening (HTVS) was performed using the SiBioLEAD platform (https://sibiolead.com/), using a ChemBridge database, which comprises approximately 850,000 molecules. Retrieved receptor structures were preprocessed using Discovery Studio Visualizer following standard protein preparation protocols[18]. The small molecule library was pre-filtered based on molecular weight (150–350 Da) and adherence to Lipinski's Rule of Five. Molecular docking was performed using AutoDock-Vina[19], integrated within the SiBioLEAD platform, to efficiently identify potential dual-target ligands.

Molecular Dynamics simulations

Molecular dynamics simulations were performed to evaluate the stability and interaction dynamics of the SBMB-004 complexes with MDM2, BD1, and BD2. These molecular dynamics simulations were executed using GROMACS[20], accessed through the SiBioLEAD molecular dynamics simulation platform[21]. For each protein-ligand complex, starting structures were preprocessed using the OPLS force field, and the complexes were placed in a solvated triclinic box filled with Simple Point Charge (SPC) water molecules[22]. To maintain ionic neutrality, sodium chloride (NaCl) was added at a physiological concentration of 0.15 mol/L. Before the production phase, the system underwent energy minimization using the steepest descent algorithm for 5 000 steps to eliminate steric clashes and optimize the initial conformation. After the system was energy-minimized, it equilibrated in two stage under constant pressure and temperature (NPT) conditions for a total of 300 ps to allow the environment to relax before initiating the production run. The subsequent molecular dynamics simulation was executed for 100 ns, with trajectory snapshots saved periodically for later analyses. Protein–ligand structural stability throughout the simulation was evaluated using root-mean-square deviation (RMSD) measurements. Additionally, binding energetics were estimated through Gibbs free energy calculations based on the Molecular Mechanics Poisson–Boltzmann Surface Area (MM/PBSA) approach[23]. These stimulations were performed to estimate the binding free energy of the complexes, providing insights into their binding affinities.

SBMB-004: compound information

SBMB-004 was identified as 1,2,3-triphenyl-1*H*-indole through a structure-guided virtual screening workflow targeting the binding sites of MDM2 and the BRD4 bromodomain. The compound was procured directly from the ChemBridge library (Cat. #5107550, ChemBridge Corporation, San Diego, CA, USA) and used without further chemical modification for all computational analyses, biochemical binding assays, and cellular experiments reported in this study. All structural representations, molecular simulations, and experimental evaluations presented herein refer to this specific chemical entity.

MDM2 time-resolved fluorescence resonance energy transfer (TR-FRET) assay

The MDM2 TR-FRET assay was performed using the commercial MDM2 TR-FRET Assay Kit (Cat. #79773, BPS Bioscience, San Diego, CA, USA) according to the manufacturer's protocol. Briefly, 10-μL reaction mixtures were prepared in 384-well white plates containing biotinylated ubiquitin, UBE1 (59 ng/μL), UBCH5b (180 ng/μL), MDM2 (7 ng/μL), ATP (4 μmol/L), and test compounds or appropriate controls (final DMSO concentration ⩽ 0.5%). Following a 3-hour incubation at 30 ℃, terbium-labeled donor and dye-labeled acceptor reagents (each diluted 1:400 in assay buffer) were added, and the plates were incubated at room temperature for an additional hour. Time-resolved fluorescence was measured using a FLUOstar Omega plate reader (BMG LABTECH, Cary, NC, USA) with excitation at 340 nm and emission detection at 620 and 665 nm (60-μs delay, 500-μs integration). The 665/620 nm emission ratios were calculated and normalized to controls to determine percent activity. The half-maximal inhibitory concentration (IC_{50}) values were derived using a four-parameter nonlinear regression model in GraphPad Prism (version 6.0).

BRD4 (BD1 and BD2) TR-FRET binding assay

The BRD4 (BD1 and BD2) TR-FRET binding assay was performed using the BRD4 (BD1 + BD2) TR-FRET Assay Kit (Cat. #32612, BPS Bioscience, San Diego, CA, USA) following the manufacturer's instructions. Briefly, 20-μL reactions were prepared in 384-well white plates containing diluted terbium donor, dye-labeled acceptor, BRD4 protein (18 ng per reaction), and test molecules or control solutions (final DMSO concentration ⩽ 0.5%). The plates were incubated for 2 h at room temperature before fluorescence measurement. TR-FRET signals were

acquired on a FLUOstar Omega time-resolved plate reader (BMG LABTECH) with excitation at 340 nm and emission detection at 620 and 665 nm (60-μs delay, 500-μs integration). Emission ratios (665/620 nm) were computed and normalized to assay controls to obtain percent activity. IC_{50} values were derived using a four-parameter nonlinear regression model in GraphPad Prism (version 6.0).

Cell culture and MTT assay

THP-1, SKM-1, and U937 acute myeloid leukemia cell lines, along with the HS-5 bone marrow stromal cell line, were obtained from the American Type Culture Collection (ATCC, Manassas, VA, USA). All cell lines were maintained in RPMI-1640 medium supplemented with 10% fetal bovine serum and antibiotics (100 U/mL penicillin and 100 U/mL streptomycin), and were cultured at 37 ℃ in a humidified incubator with 5% CO_2. Cell viability and growth were evaluated using the MTT assay as previously described[24]. Briefly, cells were plated in 96-well plates at a density of 5×10^3 cells per well and treated with SBMB-004, Nutlin-3, or JQ1 for 72 h. After treatment, MTT solution (1 mg/mL; Cat. #475989-1 GM, Sigma-Aldrich, St. Louis, MO, USA) was added to each well, and the plates were incubated for an additional 4 hours. The resulting formazan crystals were dissolved in DMSO, and absorbance was measured at 560 nm using a microplate reader (BMG LABTECH). Proliferation inhibition was calculated relative to the vehicle-treated controls, and the 50% growth inhibition (GI_{50}) values were determined by fitting the data to a nonlinear regression model in GraphPad Prism 6.0.

Intracellular p53 stabilization assay

To assess p53 dependency, SBMB-004 was evaluated in AML cell lines with distinct p53 status, including p53-wild-type (THP-1), p53-mutant (SKM-1), and p53-null (U937) models, enabling direct comparison of cellular responses across genetically defined contexts. THP-1, SKM-1, and U937 cells were treated with SBMB-004, Nutlin-3, or JQ1 at concentrations close to their respective GI_{50} values. Intracellular p53 expression was measured at 8 and 24 hours to track temporal changes in protein stabilization. After treatment, cells were washed twice with phosphate-buffered saline (PBS), fixed in 2% paraformaldehyde for 10 min at room temperature, and then permeabilized with 0.1% Triton X-100 in PBS for 10 min to facilitate antibody access to nuclear p53. After an additional wash, cells were stained with 3 μg/mL FITC-labeled anti-p53 antibody (clone DO-1, Cat. #ab270645; Abcam, Waltham, MA, USA) at 4 ℃ for 30 min in the dark. Unstained and isotype-matched controls were processed in parallel. Flow cytometric analysis was performed using a Guava easyCyte system (Millipore, Burlington, MA, USA), acquiring at least 10 000 single-cell events per sample. Flow cytometric data were analyzed using a standardized gating strategy. Briefly, cell populations were first gated based on forward scatter and side scatter parameters to exclude debris and cell aggregates. Single-cell populations were then selected to eliminate doublets. For intracellular p53 analysis, gating was defined using unstained and isotype control samples to establish background fluorescence, and p53-positive populations were quantified relative to these controls. Data were processed using InCyte software (Millipore) and expressed as the percentage of p53-positive cells relative to untreated controls. Statistical analyses and graphical representations were generated with GraphPad Prism version 6.0 (GraphPad Software, La Jolla, CA, USA).

Annexin V/Propidium Iodide (PI) apoptosis assay

Apoptosis induced by compound treatment was evaluated using Annexin V-FITC and propidium iodide (PI) dual staining. THP-1, SKM-1, and U937 cells were treated with SBMB-004, Nutlin-3, or JQ1 at concentrations approximating their respective GI_{50} values for 48 hours. Following incubation, cells were collected, washed twice with chilled PBS, and resuspended in 1× Annexin binding buffer (Cat. #V13242; Thermo Fisher Scientific, Waltham, MA, USA). Cells were stained with Annexin V-FITC and PI according to the manufacturer's instructions and incubated for 15 min at room temperature in the dark. Stained cells were immediately analyzed using a Guava easyCyte flow cytometer (Millipore), acquiring at least10000 events per sample. Data analysis employed a standardized gating strategy: debris and aggregates were excluded based on forward scatter and side scatter parameters, followed by doublet discrimination to isolate singlets. Quadrant gates were established using unstained, Annexin V-only, and PI-only controls to define fluorescence thresholds, enabling classification of cells into viable (Annexin V^-/PI^-), early apoptotic (Annexin V^+/PI^-), and late apoptotic/necrotic (Annexin V^+/PI^+) populations. Identical gating parameters were applied across all experimental conditions. Data collection and quadrant-based gating were performed using InCyte software (Millipore). Results represent the mean ± standard deviation (SD) from three independent experiments. Statistical analyses were performed

using GraphPad Prism version 6.0 (GraphPad Software, La Jolla, CA, USA).

Statistical analysis

All experiments were performed in triplicate (n = 3 independent biological replicates), and data were presented as the mean ± standard deviation (SD). Statistical analyses were conducted using GraphPad Prism version 6.0. Dose–response curves (IC_{50} and GI_{50}) were fitted using an unweighted four-parameter logistic (4PL) nonlinear regression model. Unweighted fitting was selected because plateau concentrations contained Y = 0 or SD = 0 values, which would preclude the use of relative weighted methods (*e.g.*, $1/Y^2$ or $1/SD^2$) without introducing arbitrary constants that could bias the estimation of the lower asymptote. Goodness of fit was assessed within Prism. Comparisons among multiple treatment groups were performed using one-way analysis of variance (ANOVA) followed by Tukey's multiple comparisons post hoc test. Prior to one-way ANOVA, datasets were assessed for normality and homogeneity of variances using GraphPad Prism diagnostic tools; no substantial deviations were observed, and variance distribution across treatment groups was comparable. A $P < 0.05$ was considered statistically significant. Computational docking and molecular dynamics analyses were evaluated using established scoring functions and trajectory-derived parameters, with binding free energies calculated using the MM/PBSA method.

Results

Three-dimensional structure of target proteins identifies a druggable site

To identify small molecules targeting both MDM2 and BRD4 proteins, the experimental structures of the target proteins were retrieved and evaluated for the presence of a druggable sites. The crystal structure of MDM2 bound to its reference ligand revealed a well-defined binding pocket accommodating the ligand with high shape complementarity (***Fig. 1A***). The detailed protein–ligand interaction map confirmed multiple stabilizing contacts, including hydrogen bonds and hydrophobic interactions, underscoring the ligand's tight binding to MDM2 (***Fig. 1B***). Since the BRD4 protein has two bromodomains (BD1 and BD2), both bromodomains were considered for docking analysis. The crystal structure of BRD4 bromodomain 1 (BRD4-BD1) complexed with its reference ligand demonstrated a clear binding orientation, with the ligand occupying the acetyl-lysine recognition site (***Fig. 1C***). Interaction profiling highlighted key residues forming hydrogen bonds and hydrophobic interactions with the reference ligand, suggesting favorable binding energetics (***Fig. 1D***). Similarly, BRD4 bromodomain 2 (BRD4-BD2) was retrieved and analyzed for a druggable pocket. Structural analysis of the BD2 domain revealed a conserved fold characteristic of bromodomains (***Fig. 1E***). Computational active-site prediction identified a distinct ligand-binding pocket, highlighted in green, which aligns with the canonical acetyl-lysine binding groove (***Fig. 1F***). These findings confirm the druggability of both MDM2 protein and the BRD4 bromodomains and provide structural evidence supporting their potential as therapeutic targets.

High-throughput virtual screening identifies novel lead molecules with dual interaction properties

To identify novel dual inhibitors interacting with MDM2 and BRD4 proteins, high-throughput virtual screening (HTVS) was conducted. HTVS of the ChemBridge library against MDM2 revealed a set of molecules with strong predicted binding affinities, as indicated by their docking scores (***Fig. 2A***). Most top-scoring compounds showed docking energies comparable to or better than the reference ligand, suggesting their potential as competitive MDM2 inhibitors.

Interestingly, several of these top-ranking molecules were further evaluated againstBRD4-BD1. The docking results demonstrated that a subset of the MDM2 binders also exhibited favorable binding interactions within the acetyl-lysine recognition site of BRD4-BD1 (***Fig. 2B***). A similar trend was observed when docking these compounds against BRD4-BD2. Several top candidates retained strong docking scores, confirming their binding potential across both bromodomains (***Fig. 2C***). This cross-reactivity emphasizes the structural adaptability of the identified ligands and highlights the conserved druggability of BRD4 bromodomains. The distribution of docking scores is summarized in a histogram (***Fig. 2D***), demonstrating that a significant fraction of molecules displays high binding propensities toward both MDM2 and BRD4. The 2D structures of the top lead compounds are shown in ***Supplementary Fig. 1***. These findings suggest the potential to repurpose certain MDM2-targeted compounds as multitarget inhibitors capable of simultaneously modulating the MDM2-p53 pathway and BRD4-mediated transcriptional regulation.

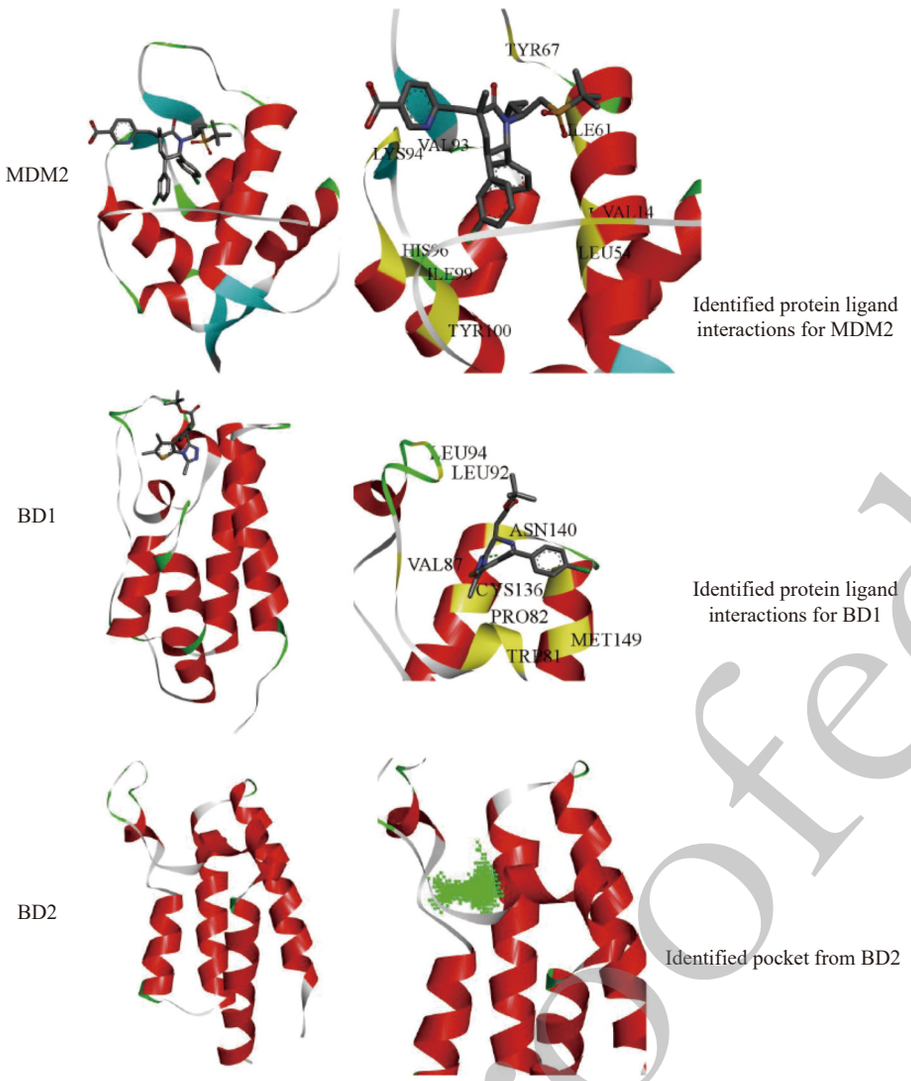

Fig. 1 **Structural modeling, docking, and binding pocket characterization of the protein–ligand complex.** A: Overall three-dimensional structure of the target protein shown in cartoon representation, highlighting the ligand bound within the predicted binding pocket. B: Enlarged view of the ligand-binding site, illustrating the docking pose of the compound and its orientation within the pocket. Key interacting residues are labeled. C: Alternative orientation of the protein structure emphasizing the helical architecture surrounding the ligand-binding region. D: Detailed protein–ligand interaction view highlighting critical residues involved in stabilizing the ligand through hydrophobic contacts and polar interactions. E: Visualization of the predicted binding pocket and spatial distribution of favorable interaction regions, shown as a green point/mesh representation within the protein cavity. F: Additional structural view of the protein, highlighting the overall topology and spatial relationship between secondary structural elements and the identified binding site.

Protein-ligand interaction profiling of top lead molecules

To identify the binding mode of the lead molecule, we performed detailed protein-ligand interaction profiling of SBMB-004 (1,2,3-triphenyl-1*H*-indole) against the target proteins. Docking of SBMB-004 into MDM2 binding pocket revealed multiple stabilizing contacts (***Fig. 3A***). Key interactions included hydrogen bonds and hydrophobic contacts with residues critical for maintaining the MDM2–p53 interface, indicating that SBMB-004 may effectively disrupt this interaction. A detailed 2D protein-ligand interaction plot illustrating the number and type of bonds between MDM2 and SBMB-004 is shown in ***Figure 3E***. When analyzed against BRD4-BD1, SBMB-004 established interactions with conserved residues lining the acetyl-lysine recognition pocket (***Fig. 3B***). These contacts suggest that the compound can be accommodated within the BD1 binding groove, supporting its potential as a dual inhibitor. Similarly, protein–ligand interaction analysis of SBMB-004 with BRD4-BD2 showed stable contacts with several pocket-lining amino acids (***Fig. 3C***, ***3F***, and ***3G***). The interaction profile in BD2 was consistent with that observed in BD1, underscoring the structural adaptability of SBMB-004 across both bromodomains. Collectively, these results demonstrate

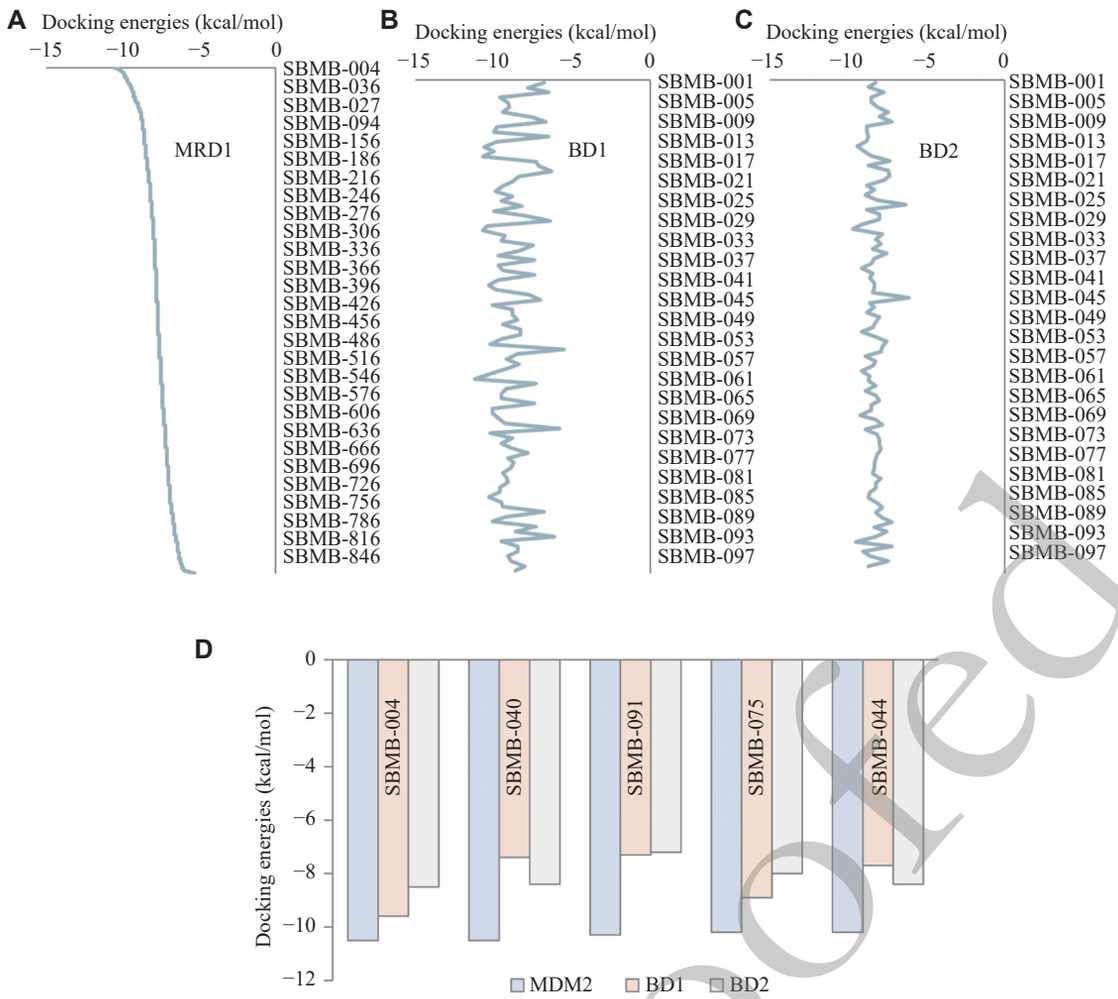

Fig. 2 **Virtual screening and cross-target docking analysis.** A: Predicted docking scores from high-throughput virtual screening of the ChemBridge library against the MDM2 protein. B: Predicted docking scores of top molecules predicted for MDM2 against the BRD4-BD1 domain. C: Predicted docking scores of top molecules predicted for MDM2 against BRD4-BD2. D: Histogram representing the predicted docking scores for top molecules showing binding affinity for both MDM2 and BRD4 domains.

that SBMB-004 engages in favorable interactions with MDM2 and both BRD4 bromodomains, highlighting its potential as a multitarget inhibitor (***Fig. 3D***). To further understand the binding efficacy of SBMB-004 relative to known inhibitors of the respective target proteins, we superimposed the predicted pose of SBMB-004 with the experimental poses of reference ligands. SBMB-004 aligned precisely within the binding pockets occupied by JQ1 in BD1 and the REL peptide in BD2 (***Supplementary Figs. 2A*** and ***3A***). Furthermore, detailed 2D interaction plots depicting the interactions between SBMB-004 and the respective reference ligands are shown in ***Supplementary Figures 2B*** and ***3B***.

Molecular dynamics simulation identifies the binding stability of SBMB-004 with target proteins

To determine the binding stability of the predicted lead molecule SBMB-004 against MDM2 and BRD4 proteins, we performed100-ns molecular dynamics simulations. For the MDM2–SBMB-004 complex, the protein backbone RMSD profile demonstrated a stable trajectory throughout the simulation, indicating minimal structural fluctuations in the presence of SBMB-004 (***Fig. 4A***). Correspondingly, the ligand RMSD stabilized below 0.25 nm, reflecting a strong and stable binding mode of SBMB-004 to the MDM2 pocket (***Fig. 4B***).

For the BRD4–SBMB-004 complexes, both the BD1 and BD2 domains were analyzed. The BD1 domain displayed overall stable RMSD values across the simulation, with no significant deviations observed in protein backbone dynamics (***Fig. 4C***), while the ligand RMSD showed limited fluctuations, supporting a stable binding conformation (***Fig. 4D***). Similarly, the BD2 domain of BRD4 exhibited consistent RMSD values for the protein (***Fig. 4E***). The ligand RMSD in the BD2 binding site stabilized after an initial

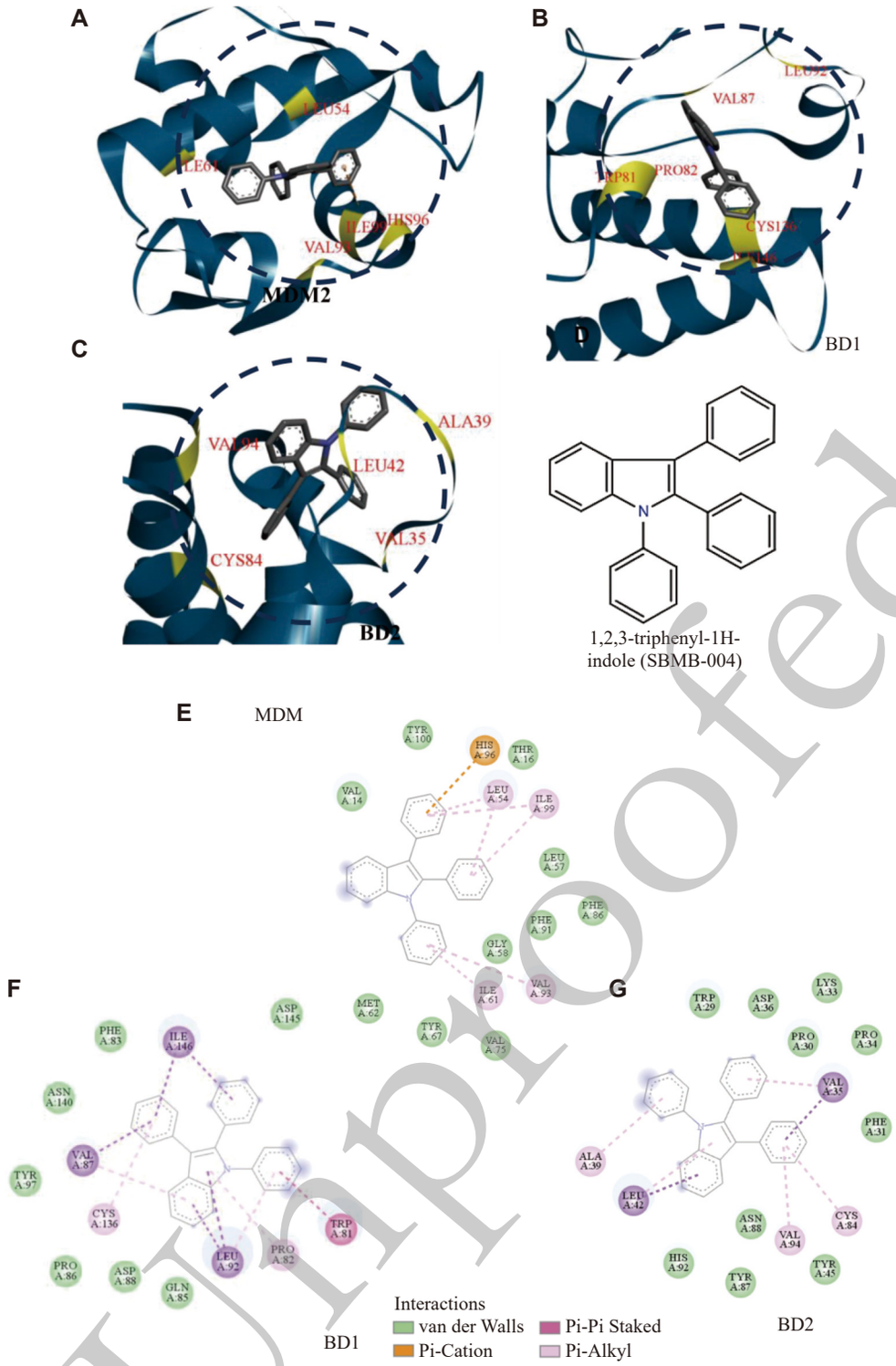

Fig. 3 **Structural and interaction profiling of SBMB-004 with MDM2 and BRD4 bromodomains.** A: Protein-ligand interaction profiling of SBMB-004 showing interactions with MDM2 amino acid residues. B: Protein-ligand interaction analysis of SBMB-004 bound to BRD4-BD1, showing interacting amino acids at the BD1 domain. C: Protein-ligand interaction analysis of SBMB-004 showing interacting amino acid residues at the BD2 domain of the BRD4 protein. D: 2D chemical structure of SBMB-004. E: Two-dimensional interaction map of SBMB-004 within the MDM2 binding site, illustrating hydrogen bonds, hydrophobic contacts, and π–π interactions with key residues. F: Two-dimensional interaction diagram of SBMB-004 bound to BRD4 bromodomain 1 (BD1), showing residue-level interactions that stabilize the ligand within the acetyl-lysine recognition pocket. G: Two-dimensional interaction diagram of SBMB-004 bound to BRD4 bromodomain 2 (BD2), highlighting conserved and distinct interaction patterns relative to BD1.

equilibration phase, further suggesting persistent interactions of SBMB-004 within the domain pocket (***Fig. 4F***). Results for individual repeats are shown in ***Supplementary Figs. 4–6***.

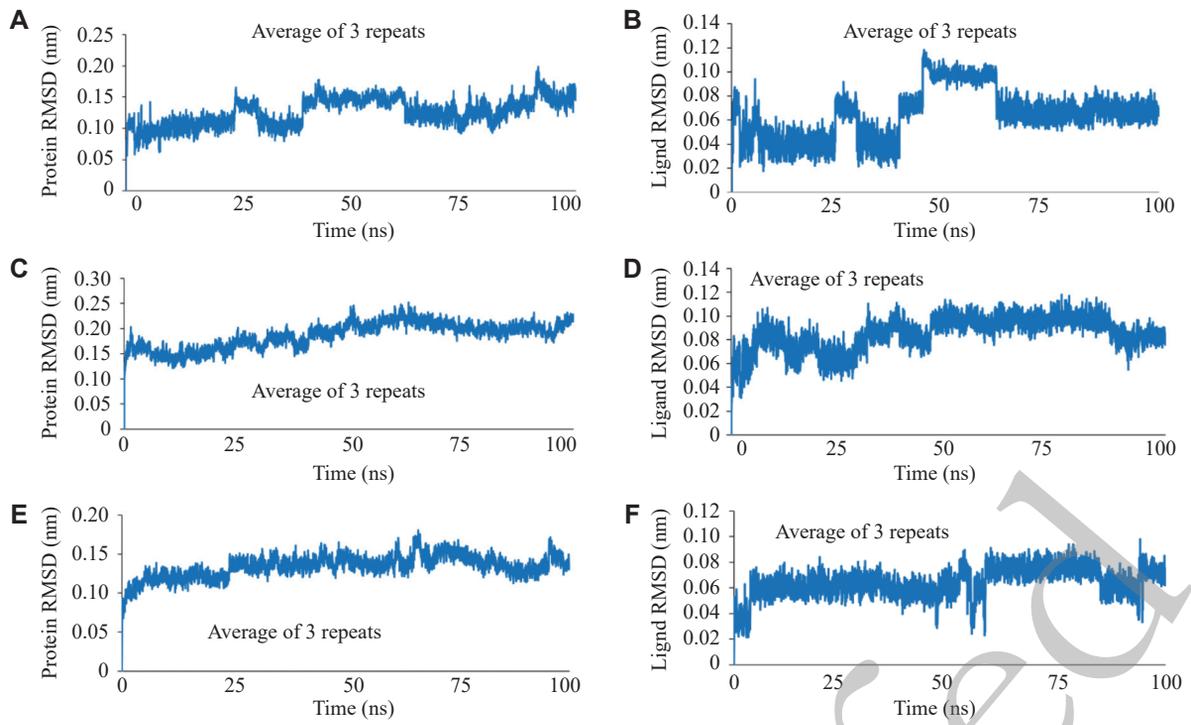

Fig. 4 **Molecular dynamics stability analysis of SBMB-004 in complex with MDM2 and BRD4 bromodomains.** A: Predicted Root Mean Square Deviation (RMSD) for the MDM2 protein when bound to SBMB-004. B: predicted ligand RMSD for SBMB-004 when bound to MDM2 protein. C: frame-by-frame RMSD for BD1 domain of BRD4 protein when bound to SBMB-004. D: predicted ligand RMSD for SBMB-004 when bound to the BD1 domain. E: predicted RMSD for the BD2 domain of BRD4 protein when bound to SBMB-004, calculated from 100 ns trajectories. F: trajectory analysis for ligand RMSD for SBMB-004 when bound to the BD2 domain of the BRD4 protein.

Collectively, these results indicate that SBMB-004 maintains stable interactions with both MDM2 and BRD4 proteins during the 100-ns simulations. The consistent RMSD values for both protein backbones and ligand trajectories confirm the structural integrity of the complexes, supporting the potential of SBMB-004 as a promising dual-target inhibitor.

Binding free energy analysis supports stable interaction of SBMB-004 with MDM2 and BRD4 domains

To further validate the stability and affinity of SBMB-004 toward MDM2 and BRD4 proteins, representative trajectory snapshots and MM/PBSA binding free energy estimates were examined. For the MDM2–SBMB-004 complex, the pre-simulation snapshot shows the initial binding pose of the ligand within the hydrophobic pocket (***Fig. 5A***). After 100 ns of MD simulation, SBMB-004 maintained its orientation in the binding site with only minimal conformational adjustments of nearby residues (***Fig. 5B***). The MM/PBSA calculations further confirmed this stability, yielding a favorable binding free energy estimate that highlights the strong affinity of SBMB-004 for MDM2 (***Fig. 5C***). For the BRD4-BD1 domain, the pre-simulation binding orientation of SBMB-004 (***Fig. 5D***) was largely preserved throughout the 100 ns trajectory, with post-simulation snapshots showing stable interactions within the acetyl-lysine recognition pocket (***Fig. 5E***). Consistently, MM/PBSA analysis predicted a favorable free energy estimate for the SBMB-004–BD1 complex, supporting its high binding stability (***Fig. 5F***).

Similarly, the BRD4-BD2 domain exhibited strong retention of SBMB-004 in the binding site across the course of the simulation. The pre- and post-simulation snapshots (***Fig. 5G*** and ***5H***) indicate that the ligand remained well-anchored within the binding cavity, with minor adjustments accommodating protein flexibility. The MM/PBSA predicted binding free energy further validated the favorable interaction between SBMB-004 and BD2 (***Fig. 5I***).

Overall, the combined trajectory snapshots and MM/PBSA analyses strongly support that SBMB-004 forms stable and energetically favorable interactions with both MDM2 and BRD4 (BD1 and BD2 domains), reinforcing its potential as a dual-target inhibitor.

Inhibition of MDM2 and BRD4 by SBMB-004

To directly assess biochemical target engagement, SBMB-004 was evaluated using TR-FRET-based

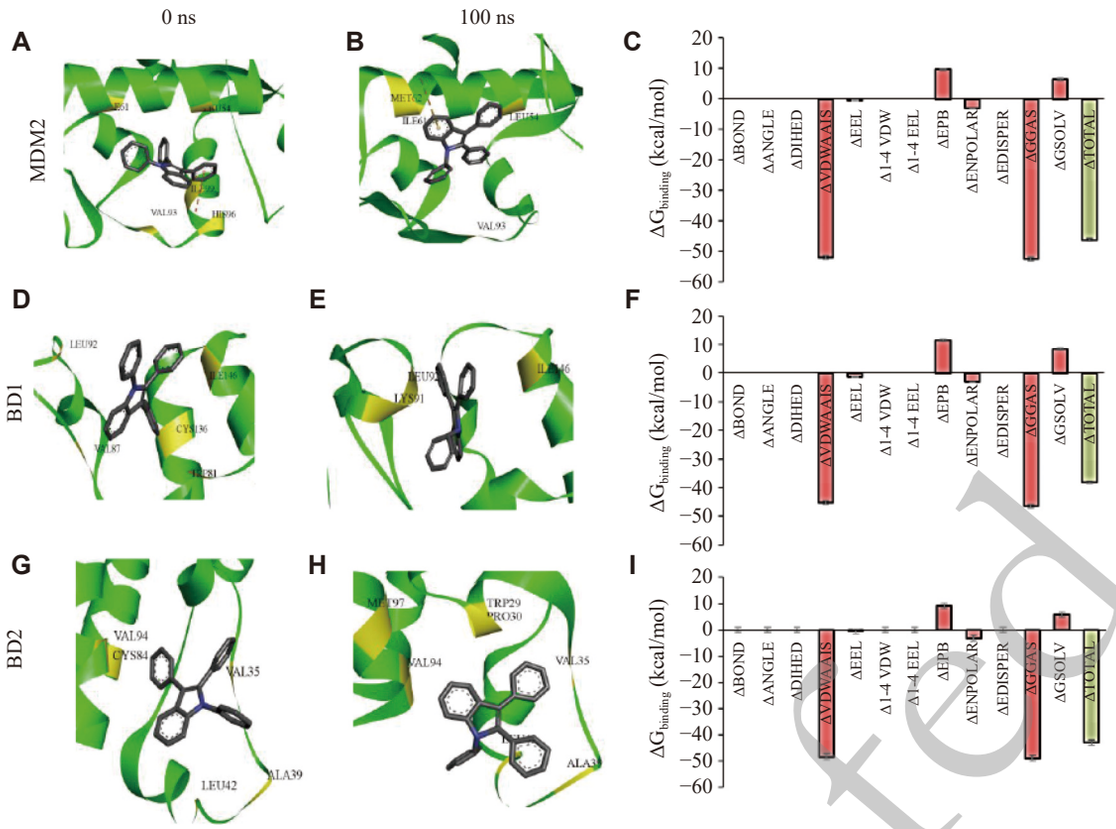

Fig. 5 **Molecular dynamics snapshots and MM/PBSA binding free energy analysis of SBMB-004 with MDM2 and BRD4 bromodomains.** A: Snapshot of the trajectory frame before the simulation for MDM2 bound to SBMB004. B: Snapshot of the trajectory frame after the simulation (100 ns) for MDM2 bound to SBMB-004. C: MM/PBSA predicted the binding free energy estimate for SBMB-004 with MDM2. D: Snapshot of the trajectory frame before the simulation for BRD4-BD1 bound to SBMB004. E: Snapshot of trajectory frame after the simulation (100 ns) for BRD4-BD1 bound to SBMB-004. F: MM/PBSA predicted binding free energy estimate for SBMB-004 with BRD4-BD1. G:Snapshot of the trajectory frame before the simulation for BRD4-BD2 bound to SBMB004. H: Snapshot of the trajectory frame after the simulation (100 ns) for BRD4-BD2 bound to SBMB-004. I: MM/PBSA predicted binding free energy estimate for SBMB-004 with BRD4-BD2.

binding assays against recombinant MDM2 and BRD4 bromodomain proteins, providing quantitative IC_{50} values that confirm direct protein–ligand interactions at both targets. The compound demonstrated potent inhibition of MDM2 with an IC_{50} value of 80.08 nmol/L, and BRD4 (BD1 + BD2) with an IC_{50} value of 95.15 nmol/L (***Fig. 6A*** and ***6B***). These values are comparable to, or improved upon, those of standard reference inhibitors (Nutlin-3 for MDM2: IC_{50} = 108.8 nmol/L; JQ1 for BRD4: IC_{50} = 90.49 nmol/L) (***Fig. 6C*** and ***6D***).

Anti-proliferative effects of SBMB-004 in AML cell models

SBMB-004 demonstrated potent and selective anti-proliferative activity across AML cell models in a dose-dependent manner, as determined by the MTT assay. Following 48 h of treatment, SBMB-004 significantly reduced cell viability in all AML lines tested, with calculated GI_{50} values of 110.9 nmol/L for THP-1 (p53 wild-type), 356.1 nmol/L for SKM-1 (p53 mutant), and 1 753 nmol/L for U937 (p53-null). In contrast, the non-malignant bone marrow stromal cell line HS-5 exhibited a GI_{50} of 3 605 nmol/L (***Fig. 7A–7D***). This pronounced differential sensitivity underscores the compound's selectivity for malignant hematopoietic cells over normal stromal counterparts.

Comparative analysis with pathway-specific reference inhibitors revealed distinct potency profiles. The MDM2 inhibitor Nutlin-3 showed comparatively higher GI_{50} values of 985.2 nmol/L, 1879 nmol/L, and 4 120 nmol/L in THP-1, SKM-1, and U937 cells, respectively (***Fig. 7A–7C***), indicating less efficient cytotoxicity at equivalent time points. The BRD4 inhibitor JQ1 exhibited intermediate activity, with GI_{50} values of 220.2 nmol/L in THP-1, 279.3 nmol/L in SKM-1, and 1 025 nmol/L in U937 (***Fig. 7A–7C***). In the normal HS-5 line, Nutlin-3 and JQ1 demonstrated minimal cytotoxic effects, with GI_{50} values of 4 418 nmol/L and 1874 nmol/L, respectively (***Fig. 7D***).

Together, these results confirm that SBMB-004

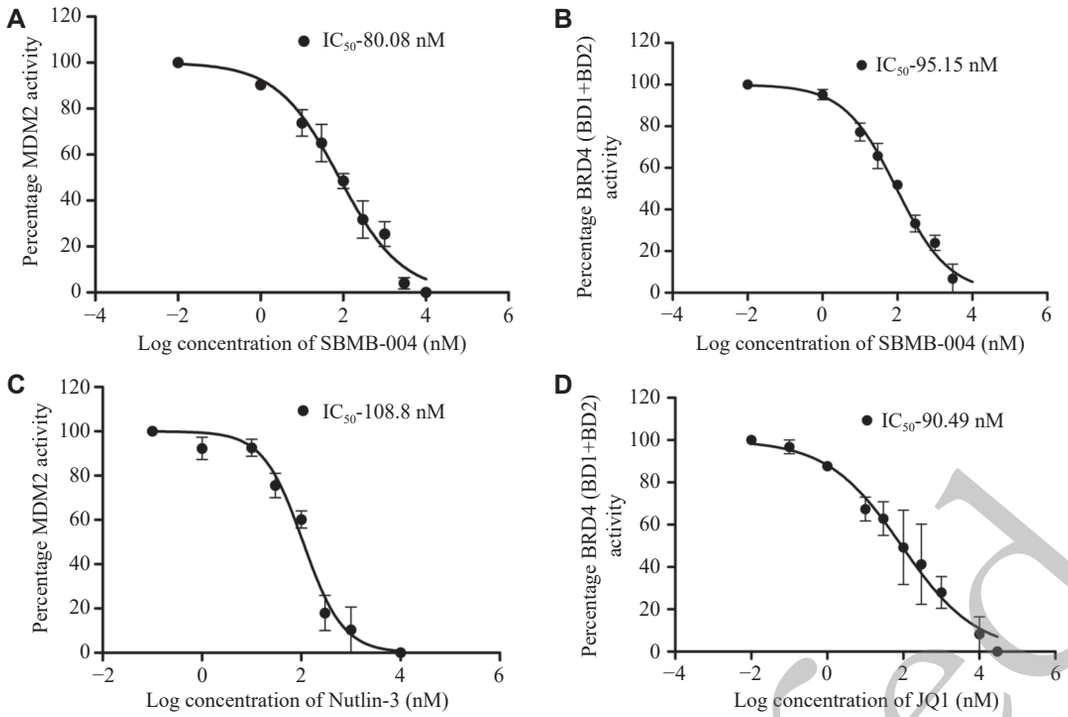

Fig. 6 **Inhibition of MDM2 and BRD4 by SBMB-004 compared with standard inhibitors.** TR-FRET binding assays were performed to evaluate the inhibitory activity of SBMB-004. A: Inhibition of MDM2 by SBMB-004. B: Inhibition of BRD4 (BD1+BD2) by SBMB-004. C: Inhibition of MDM2 by the reference compound Nutlin-3. D: Inhibition of BRD4 (BD1 + BD2) by the reference compound JQ1. Data are presented as mean ± SD from three independent experiments performed in triplicate. Nonlinear regression curve fitting was conducted using a four-parameter logistic model in GraphPad Prism software (version 6.0).

exhibits superior anti-leukemic potency compared to established single-target inhibitors. The efficacy profile correlates with p53 functional status: highest sensitivity was observed in p53-competent THP-1 cells, while reduced efficacy was noted in p53-defective or null lines. The minimal activity against HS-5 cells further supports the favorable therapeutic selectivity of SBMB-004.

Time-dependent stabilization of p53

To confirm MDM2 inhibition and downstream activation of the p53 pathway, intracellular p53 expression was quantified by flow cytometry after 8 h and 24 h of compound exposure. In THP-1 cells, treatment with SBMB-004 led to a marked and time-dependent increase in p53-positive cells, rising from 8.04% ± 3.84% (control) to 20.14% ± 4.37% at 8 h, and from 9.16% ± 2.55% (control) to 41.89% ± 3.89% at 24 h (***Fig. 8A***). This corresponds to an approximately 2.0-fold and 4.5-fold elevation in intracellular p53 levels relative to untreated controls. These effects were comparable to those observed with the reference MDM2 inhibitor Nutlin-3, which yielded 34.50% ± 5.11 % and 52.55% ± 6.78 % p53-positive cells at 8 h and 24 h, respectively (***Fig. 8A***).

In SKM-1 cells, which harbor mutant p53, SBMB-004 produced only modest increases in p53-positive populations—9.76% ± 3.38% at 8 h and 20.11% ± 3.97% at 24 h—relative to their corresponding controls (6.13% ± 2.17% and 7.01% ± 2.61%, respectively) (***Fig. 8B***). Similarly, Nutlin-3 induced a limited rise (8.81% ± 1.58% at 8 h and 15.57% ± 2.85% at 24 h), consistent with stabilization of non-functional mutant p53 protein.

In contrast, U937 cells, which lack functional p53, displayed no appreciable change in p53 staining upon treatment with either SBMB-004 or Nutlin-3, confirming the specificity of p53 reactivation in wild-type contexts (***Fig. 8C***). As expected, the BRD4 inhibitor JQ1 did not alter intracellular p53 levels in any of the tested cell lines, thereby validating assay specificity.

Collectively, these data demonstrate that SBMB-004 induces time-dependent stabilization of intracellular p53 in p53-competent AML cells, closely paralleling the effects of Nutlin-3. The modest response in SKM-1 and absence of activation in U937 further highlight the dependence of this effect on p53 functional integrity, supporting the dual MDM2/BRD4 inhibition mechanism at the cellular level.

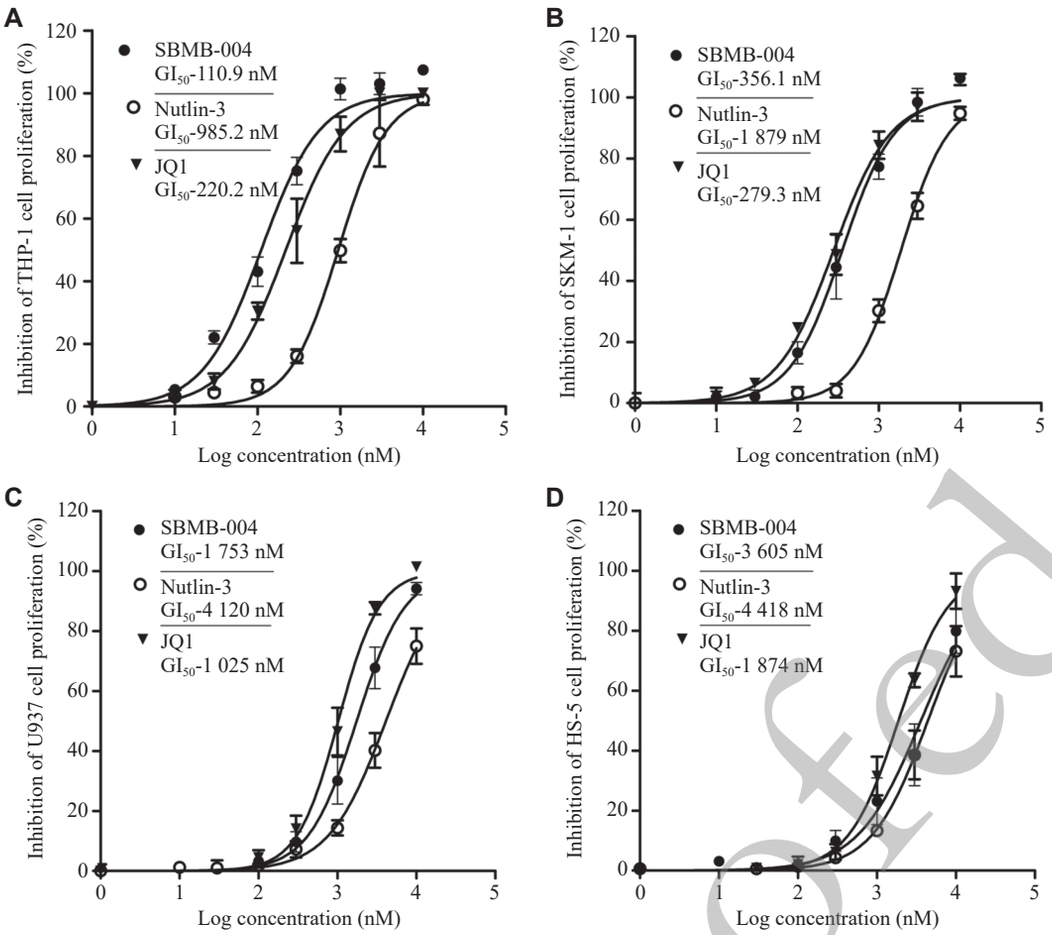

Fig. 7 **Dose-dependent anti-proliferative activity of SBMB-004 in AML models.** A: THP-1, B: SKM-1, C: U937, and D: HS-5 cells were treated for 48 h with increasing concentrations of SBMB-004, Nutlin-3, or JQ1, and cell viability was measured using the MTT assay. Data represent mean ± SD (n = 3 independent experiments). GI_{50} values were calculated from nonlinear regression fits in GraphPad Prism software (version 6.0).

Induction of apoptosis by SBMB-004 *via* Annexin V/PI

Annexin V/PI flow cytometric analysis performed after 48 h of treatment revealed apoptosis patterns consistent with the cytotoxicity and p53 activation profiles observed in preceding assays. At their respective GI_{50} concentrations, SBMB-004 induced significant apoptosis in AML cells, with 32.46% ± 5.37% apoptotic cells in THP-1, 21.05% ± 4.57% in SKM-1, and only 9.23% ± 1.36% in U937 (***Fig. 9A–9C***). The apoptotic response in THP-1 cells — harboring wild-type p53 —was notably stronger than in p53-mutant or p53-null models, consistent with p53-dependent cytotoxicity.

In comparison, the reference MDM2 inhibitor Nutlin-3 induced 37.37% ± 4.58%, 5.77% ± 2.26%, and 6.72% ± 2.57% apoptosis in THP-1, SKM-1, and U937 cells, respectively (***Fig. 9A–9C***), further confirming the dependence of MDM2-mediated apoptosis on intact p53 signaling. The BRD4 inhibitor JQ1 displayed a distinct profile, eliciting 22.98% ± 4.85% apoptosis in THP-1, 30.79% ± 3.33% in SKM-1, and 19.34% ± 2.89% in U937, suggesting effective induction of BRD4-dependent apoptosis irrespective of p53 status (***Fig. 9A–9C***).

Together, these findings suggest that SBMB-004 promotes apoptosis through dual mechanisms: p53-dependent activation in p53-competent cells and BRD4-mediated transcriptional suppression in p53-deficient or null backgrounds. The preferential apoptotic response observed in AML-derived cell lines, compared to the minimal effects in non-malignant controls, further reinforces the compound's selective anti-leukemic potential.

Discussion

In AML, therapeutic outcomes remain compromised by high relapse rates, driven largely by the rapid upregulation of survival pathways that blunt p53-mediated apoptosis and sustain oncogenic

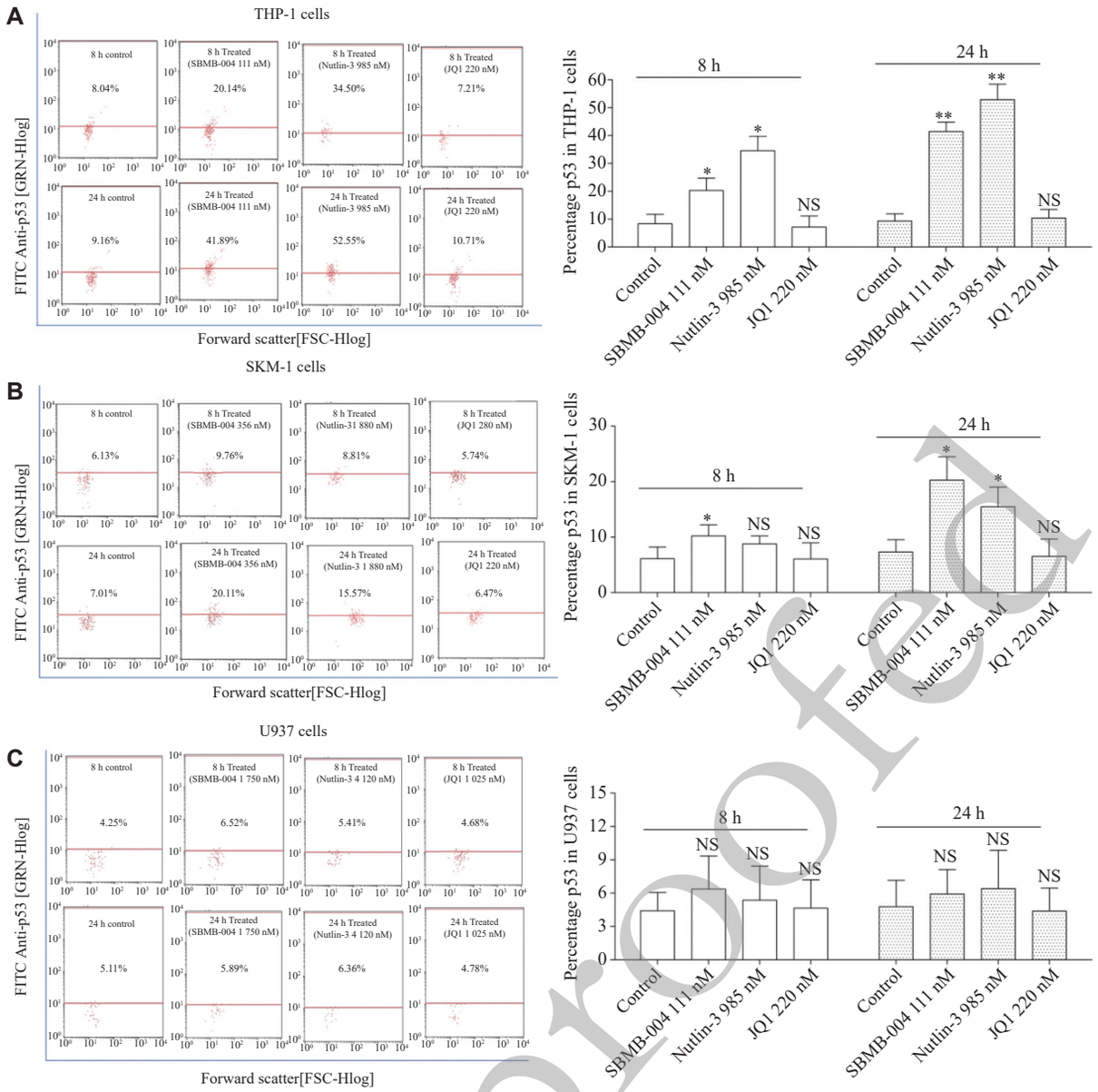

Fig. 8 **Time-dependent stabilization of p53 following SBMB-004 treatment.** Intracellular p53 expression was quantified by flow cytometry after 8 h and 24 h exposure to SBMB-004 or reference inhibitors at their respective GI_{50} concentrations in A: THP-1, B: SKM-1, and C: U937 cells. For each panel, the flow cytometry scatter plot represents a single representative experiment, with values indicating the percentage of p53-positive cells. The accompanying bar graph adjacent to each scatter plot summarizes data from three independent biological experiments (n = 3) and is presented as mean ± SD. Flow cytometry data were analyzed using InCyte software (Millipore). Statistical significance was determined using one-way analysis of variance (ANOVA) followed by Tukey's post hoc test, with significance thresholds indicated as *$p < 0.05$ and **$p < 0.01$; NS denotes not significant.

transcriptional programs, including *MYC*. MDM2 acts as a negative regulator of the tumor suppressor p53[25], while BRD4 functions as a transcriptional coactivator implicated in oncogene expression[26]. Consequently, dual inhibition could promote the restoration of p53 function while suppressing oncogenic transcription, potentially offering broader anticancer efficacy than single-target inhibition[27]. Targeting both MDM2 and BRD4 simultaneously represents a rational therapeutic strategy, as these proteins regulate critical but distinct pathways in cancer progression[28].

The present study integrates structure-based screening, molecular dynamics simulations, and binding free energy calculations to identify and characterize SBMB-004 as a potential dual-target inhibitor of MDM2 and BRD4 proteins for AML[23]. The availability of high-resolution experimental structures for MDM2 and BRD4 bromodomains enabled precise identification of druggable sites and provided a robust foundation for docking and simulation studies[10]. Our structural analyses confirmed that both MDM2 and BRD4 bromodomains

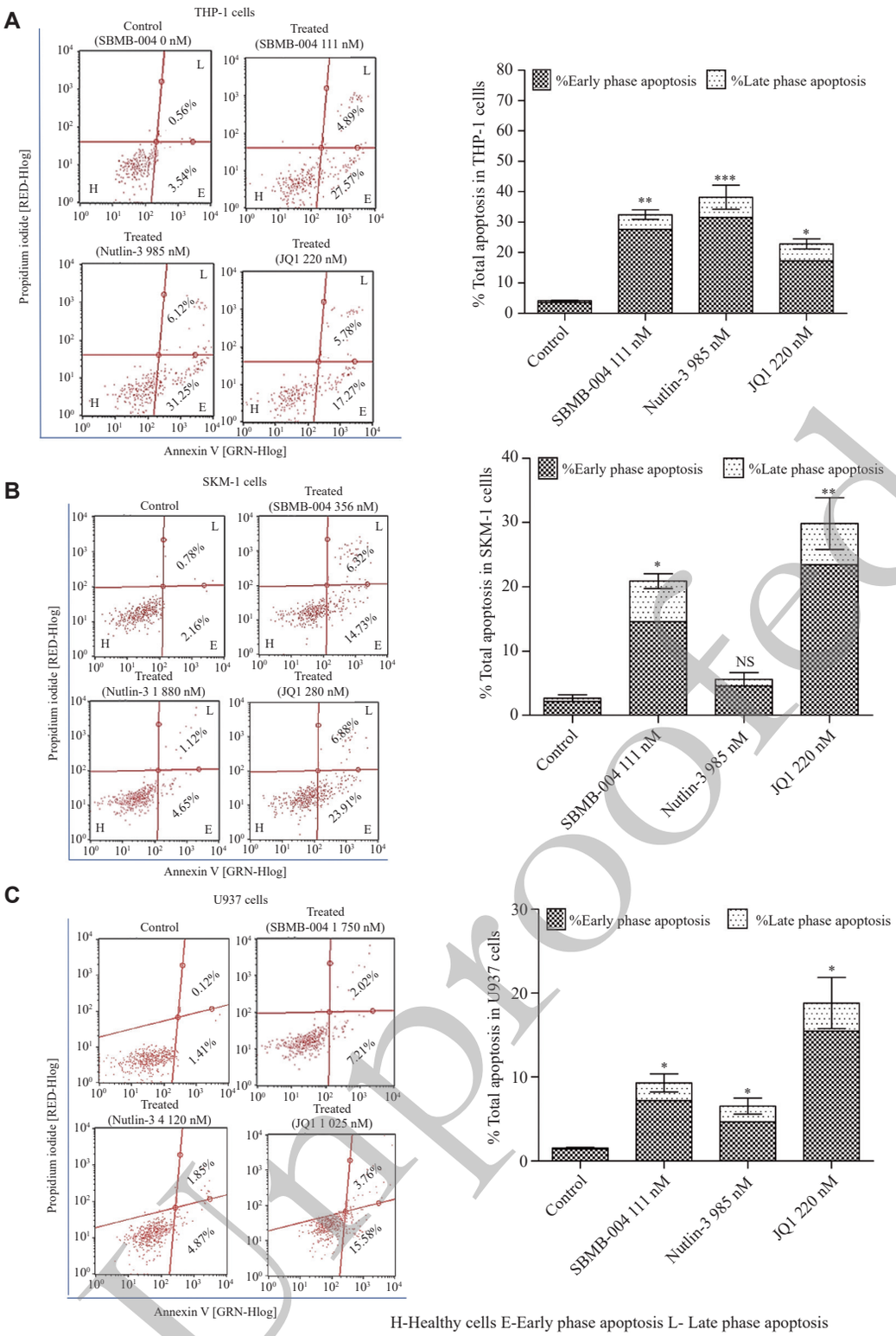

Fig. 9 **SBMB-004 induces apoptosis in AML cells.** Annexin V–FITC/propidium iodide (PI) staining was performed after 48 h treatment with SBMB-004 or reference inhibitors at their respective GI_{50} concentrations in A: THP-1, B: SKM-1, and C: U937 cells. For each panel, the flow cytometry dot plot represents a single representative experiment, with quadrant values indicating the percentage of apoptotic cells. Total apoptosis was calculated as the sum of early (Annexin V^+/PI^-) and late (Annexin V^+/PI^+) apoptotic populations. The accompanying bar graph adjacent to each dot plot summarizes total apoptotic fractions from three independent biological experiments (n = 3) and is presented as mean ± SD. Apoptotic populations were quantified using a consistent Annexin V/PI quadrant gating strategy applied uniformly across all samples. Flow cytometry data were analyzed using InCyte software (Millipore). Statistical significance was determined using one-way analysis of variance (ANOVA) followed by Tukey's post hoc test, with significance thresholds indicated as *p < 0.05 and **p < 0.01; NS denotes not significant.

possess well-defined binding pockets with high shape complementarity, supporting their suitability as therapeutic targets[6].

High-throughput virtual screening of the ChemBridge library identified multiple candidate molecules with favorable docking scores against MDM2. Remarkably, a subset of these top-ranking molecules also displayed strong binding potential for both BRD4 bromodomains, indicating that structural features conducive to MDM2 binding may also be compatible with the BRD4-BD1 pocket, supporting the possibility of dual-target inhibition[11]. Among these candidates, SBMB-004 emerged as the most promising lead, exhibiting consistently high docking scores across all three targets. Protein–ligand interaction profiling further revealed that SBMB-004 engages key residues at the MDM2–p53 interface and within the acetyl-lysine recognition grooves of BRD4, indicating that it may effectively interfere with both protein–protein interactions and epigenetic regulatory functions[29].

Molecular dynamics simulations were performed to evaluate interaction stability under physiologically relevant conditions. RMSD analyses indicated stable binding of SBMB-004 to MDM2, BRD4-BD1, and BRD4-BD2 over 100 ns trajectories, with minimal fluctuations in protein backbones and ligand orientations. These observations suggest that SBMB-004 can accommodate structurally distinct binding pockets while maintaining stable interactions, a desirable feature for multitarget inhibitors.[30][31].

Binding free energy analysis using MM/PBSA further reinforced these findings. SBMB-004 demonstrated favorable binding free energy estimates across all three targets, consistent with strong and stable interactions[18]. The alignment of favorable docking scores, stable MD trajectories, and supportive binding free energy values provides compelling evidence for the robustness of SBMB-004's binding profile. These results not only validate the computational pipeline employed but also underscore the therapeutic potential of SBMB-004 as a dual inhibitor[14].

SBMB-004 represents a rationally designed, first-in-class dual MDM2/BRD4 inhibitor that concurrently restores p53 signaling and suppresses BRD4-driven oncogenic transcription. The integrated computational, biochemical, and cell-based evidence presented herein demonstrates the compound's capacity to engage both molecular targets effectively. High-affinity binding, predicted by molecular docking and validated by TR-FRET enzymatic assays, translated into potent cellular activity, evidenced by nanomolar GI_{50} values across AML cell lines. p53 dependency was investigated by evaluating SBMB-004 in AML cell lines with distinct p53 backgrounds—wild-type (THP-1), mutant (SKM-1), and null (U937)—facilitating direct assessment of genotype-dependent cellular responses. In p53-competent THP-1 cells, SBMB-004 treatment was associated with increased intracellular p53 levels within 24 h, comparable to the reference MDM2 inhibitor Nutlin-3 at lower concentrations, suggesting improved cellular uptake and potential contribution from BRD4 inhibition. Treatment with SBMB-004 also corresponded with induction of apoptosis in THP-1 cells, consistent with p53-mediated transcriptional activation of pro-apoptotic factors such as BAX and PUMA and engagement of mitochondrial apoptotic pathways.[32].

In SKM-1 cells, which harbor mutant p53, SBMB-004 elicited modest p53 accumulation (approximately two-fold over control) but still induced approximately 21% apoptosis, suggesting that apoptosis in this context is likely mediated through BRD4 suppression and subsequent downregulation of *MYC* and *BCL2*, both recognized transcriptional targets of BRD4. This pattern mirrors reports that BRD4 inhibition triggers apoptosis independent of p53 status by disrupting super-enhancer-driven transcription in AML[33].

In U937 cells lacking functional p53, SBMB-004 did not increase intracellular p53 levels yet still induced a modest apoptotic response (~9%), comparable to that observed with JQ1, indicating that BRD4-mediated transcriptional suppression can drive cell death independently of p53. Differences in the activity profiles of Nutlin-3 and JQ1 across these models further emphasize the distinct and complementary roles of MDM2 and BRD4 inhibition. The capacity of SBMB-004 to promote apoptosis in both p53-intact and p53-deficient contexts supports its classification as a dual-acting agent and suggests potential to overcome resistance associated with p53 pathway loss in AML [34]. Although this study primarily established dual target engagement and functional cellular effects, further characterization of downstream molecular responses would enhance mechanistic clarity. Evaluation of canonical p53 targets, such as CDKN1A (p21), PUMA, and BAX, alongside BRD4-regulated oncogenic drivers including MYC, BCL2, and CDK6, would provide greater insight into pathway modulation and dose-dependent responses. Nonetheless, the observed patterns of p53 stabilization and apoptosis are consistent with known mechanisms of MDM2 and BRD4 inhibition.

From a therapeutic perspective, concurrent targeting

of MDM2 and BRD4 addresses two key vulnerabilities in AML. Inhibition of MDM2 stabilizes p53 by blocking its ubiquitination and degradation, thereby enabling activation of downstream tumor suppressor programs, while BRD4 inhibition suppresses transcriptional networks that support proliferation and survival. Through simultaneous activation of tumor suppressive pathways and repression of oncogenic signaling, SBMB-004 represents a multitarget strategy aligned with emerging approaches that aim to enhance efficacy beyond single-pathway inhibition [32][35][36].

The selectivity of SBMB-004 toward AML cells, sparing HS-5 stromal cells (GI_{50} > 3.6 μmol/L), further highlights its therapeutic potential and reduced off-target toxicity. This preferential cytotoxicity likely reflects differential dependency of leukemic cells on BRD4-mediated transcription and MDM2-driven p53 turnover, both of which are dysregulated in AML but largely quiescent in normal stromal cells. Collectively, these results position SBMB-004 as a promising prototype for developing multi-functional inhibitors capable of overcoming both genotypic and epigenetic resistance in AML.

In summary, this study integrates structure-based computational screening with biochemical and cellular validation to establish SBMB-004 as a proof-of-concept dual MDM2/BRD4 inhibitor in AML. Molecular docking and focused molecular dynamics analyses supported stable ligand engagement, with RMSD convergence indicating consistent complex stability; given that these predictions were corroborated experimentally, simulations were intentionally limited and did not include extended timescales, replicate trajectories, or additional conformational metrics. The observed dual targeting of BRD4 BD1 and BD2 likely arises from conserved features of the acetyl-lysine binding pocket and the ligand's adaptable scaffold, although detailed domain-specific determinants will require further SAR and 3D-QSAR investigation. While the current findings demonstrate p53 stabilization and apoptosis as functional evidence of pathway engagement, additional transcriptional and protein-level analyses of key downstream targets, along with evaluation of phosphorylated or nuclear p53, would provide greater mechanistic resolution. Expanding studies to include dose- and time-dependent profiling, primary AML samples, and patient-derived models will further strengthen translational relevance. Future efforts will focus on comprehensive pathway characterization, extended and replicated molecular dynamics simulations to capture ligand-induced conformational dynamics, and in vivo evaluation in AML models to assess pharmacokinetics, safety, and therapeutic efficacy, thereby advancing the development of dual-target strategies.

SBMB-004 represents a novel dual-target therapeutic strategy that concurrently engages MDM2 and BRD4, addressing two critical and complementary drivers of AML pathogenesis. By simultaneously restoring tumor suppressor function and disrupting oncogenic transcriptional programs, this approach offers a mechanistically integrated framework to overcome key resistance pathways, including p53 inactivation. The capacity of a single small molecule to modulate both axes highlights a shift toward multitarget design as a means to enhance therapeutic efficacy and durability. Collectively, these findings position dual MDM2/BRD4 inhibition as a promising and clinically relevant direction for the development of next-generation therapies in AML and related malignancies..

Funding

The author extends their appreciation to the Deanship of Scientific Research at King Khalid University for funding this work through Small Research Groups under grant number RGP.1/278/44.

Acknowledgments

The Authors express their gratitude to SMARTBIO LABS, Chennai-78, Tamil Nadu, India for help with data processing, and SiBIOLEAD, Little Rock, Arkansas, USA, for providing server space for software for HTVS, and MD simulations rendered in this study.

Author contributions

Mohammad Abohassan: Funding acquisition, investigation, validation, and writing—original draft preparation. **Mesfer Alshahrani:** Methodology, formal analysis, and data curation. **Prasanna Rajagopalan:** Conceptualization, resources, supervision, writing—review and editing, and project administration.

References

[1] Pollyea DA, Altman JK, Assi R, et al. Acute myeloid leukemia, version 3.2023, NCCN clinical practice guidelines in oncology[J]. *J Natl Compr Canc Netw*, 2023, 21(5):

503–513.

[2] Sidhu J, Gogoi MP, Krishnan S, et al. Relapsed acute lymphoblastic leukemia[J]. *Indian J Pediatr*, 2024, 91(2): 158–167.

[3] Dozzo A, Galvin A, Shin JW, et al. Modelling acute myeloid leukemia (AML): What's new? A transition from the classical to the modern[J]. *Drug Deliv Transl Res*, 2023, 13(8): 2110–2141.

[4] Mijit M, Caracciolo V, Melillo A, et al. Role of p53 in the regulation of cellular senescence[J]. *Biomolecules*, 2020, 10(3): 420.

[5] Brummer T, Zeiser R. The role of the MDM2/p53 axis in antitumor immune responses[J]. *Blood*, 2024, 143(26): 2701–2709.

[6] Sparks A, Dayal S, Das J, et al. The degradation of p53 and its major E3 ligase Mdm2 is differentially dependent on the proteasomal ubiquitin receptor S5a[J]. *Oncogene*, 2014, 33(38): 4685–4696.

[7] Zhu H, Gao H, Ji Y, et al. Targeting p53-MDM2 interaction by small-molecule inhibitors: Learning from MDM2 inhibitors in clinical trials[J]. *J Hematol Oncol*, 2022, 15(1): 91.

[8] Huang Y, Li W, Zhou Y, et al. Strategies for p53 activation and targeted inhibitors of the p53-Mdm2/MdmX interaction[J]. *Cells*, 2025, 14(8): 583.

[9] Kühn MWM, Pemmaraju N, Heidel FH. The evolving landscape of epigenetic target molecules and therapies in myeloid cancers: Focus on acute myeloid leukemia and myeloproliferative neoplasms[J]. *Leukemia*, 2025, 39(8): 1824–1837.

[10] Liu Z, Wang P, Chen H, et al. Drug discovery targeting bromodomain-containing protein 4[J]. *J Med Chem*, 2017, 60(11): 4533–4558.

[11] Kotekar A, Singh AK, Devaiah BN. BRD4 and MYC: Power couple in transcription and disease[J]. *FEBS J*, 2022, 290(20): 4820–4842.

[12] Roe JS, Vakoc CR. The essential transcriptional function of BRD4 in acute myeloid leukemia[J]. *Cold Spring Harb Symp Quant Biol*, 2016, 81: 61–66.

[13] Labrie M, Brugge JS, Mills GB, et al. Therapy resistance: Opportunities created by adaptive responses to targeted therapies in cancer[J]. *Nat Rev Cancer*, 2022, 22(6): 323–339.

[14] Wang W, Du Y, Datta S, et al. Targeting the MYCN-MDM2 pathways for cancer therapy: Are they druggable?[J]. *Genes Dis*, 2025, 12(2): 101156.

[15] Lei ZN, Tian Q, Teng QX, et al. Understanding and targeting resistance mechanisms in cancer[J]. *MedComm*, 2023, 4(3): e265.

[16] Jonas BA, Medeiros BC. Individualizing therapeutic strategies in acute myeloid leukemia: Moving beyond the 'one-size-fits-all' approach[J]. *Oncology*, 2016, 30(4): 330–333.

[17] Gonzalez AZ, Li Z, Beck HP, et al. Novel inhibitors of the MDM2-p53 interaction featuring hydrogen bond acceptors as carboxylic acid isosteres[J]. *J Med Chem*, 2014, 57(7): 2963–2988.

[18] Tshongo C, Baguma M, Mateso GQ, et al. Hyperglycemia and elevated C-reactive protein are independent predictors of hospital mortality in hospitalized COVID-19 patients in South-Kivu, eastern Democratic Republic of the Congo: A cross-sectional study[J]. *Health Sci Rep*, 2024, 7(1): e1803.

[19] Trott O, Olson AJ. AutoDock Vina: Improving the speed and accuracy of docking with a new scoring function, efficient optimization, and multithreading[J]. *J Comput Chem*, 2010, 31(2): 455–461.

[20] Van Der Spoel D, Lindahl E, Hess B, et al. GROMACS: Fast, flexible, and free[J]. *J Comput Chem*, 2005, 26(16): 1701–1718.

[21] Utami PD, Setianingsih H, Sari DRT. In silico approach triterpene glycoside of *H. atra* Targeting orotidine 5-monophosphate decarboxylase protein (PfOMPDC) in *P. falciparum* infection mechanism[J]. *Biomed Res Int*, 2024, 2024: 5924799.

[22] Abohassan M, Alshahrani M, Alshahrani MY, et al. Insilco and Invitro approaches identify novel dual PI3K/AKT pathway inhibitors to control acute myeloid leukemia cell proliferations[J]. *Med Oncol*, 2022, 39(12): 249.

[23] Valdés-Tresanco MS, Valdés-Tresanco ME, Valiente PA, et al. gmx_MMPBSA: A new tool to perform end-state free energy calculations with GROMACS[J]. *J Chem Theory Comput*, 2021, 17(10): 6281–6291.

[24] Al Shahrani M, Abohassan M, Alshahrani M, et al. Identification of 8-(2-methyl phenyl)-9H-benzo[f]indeno[2, 1-c]quinolin-9-one (C-5635020) as a novel and selective TGFβ RII kinase inhibitor for breast cancer therapy[J]. *Biochem Biophys Res Commun*, 2025, 746: 151225.

[25] Tu Y, Gao X, Li G, et al. MicroRNA-218 inhibits glioma invasion, migration, proliferation, and cancer stem-like cell self-renewal by targeting the polycomb group gene *Bmi1*[J]. *Cancer Res*, 2013, 73(19): 6046–6055.

[26] Dawson MA, Prinjha RK, Dittmann A, et al. Inhibition of BET recruitment to chromatin as an effective treatment for MLL-fusion leukaemia[J]. *Nature*, 2011, 478(7370): 529–533.

[27] Latif AL, Newcombe A, Li S, et al. BRD4-mediated repression of p53 is a target for combination therapy in AML[J]. *Nat Commun*, 2021, 12(1): 241.

[28] Loftus JC, Dhruv H, Tuncali S, et al. TROY (TNFRSF19) promotes glioblastoma survival signaling and therapeutic resistance[J]. *Mol Cancer Res*, 2013, 11(8): 865–874.

[29] Alghamdi MA, Deshpande H. Dual targeting of MEK1 and Akt kinase identified SBL-027 as a promising lead candidate to control cell proliferations in gastric cancer[J]. *Biotechnol Appl Biochem*, 2025, 72(4): 1006–1017.

[30] Hushmandi K, Imani Fooladi AA, Reiter RJ, et al. Next-generation immunotherapeutic approaches for blood cancers: Exploring the efficacy of CAR-T and cancer vaccines[J]. *Exp Hematol Oncol*, 2025, 14(1): 75.

[31] Emiroglu M, Karaali C, Salimoglu S, et al. Oncoplastic

reduction mammoplasty for breast cancer in women with macromastia: Long term aesthetic, functional and satisfaction outcomes[J]. *Contemp Oncol (Pozn)*, 2016, 20(3): 256–260.

[32] Kojima K, Konopleva M, McQueen T, et al. Mdm2 inhibitor Nutlin-3a induces p53-mediated apoptosis by transcription-dependent and transcription-independent mechanisms and may overcome Atm-mediated resistance to fludarabine in chronic lymphocytic leukemia[J]. *Blood*, 2006, 108(3): 993–1000.

[33] Ali K, Soond DR, Piñeiro R, et al. Inactivation of PI(3)K p110δ breaks regulatory T-cell-mediated immune tolerance to cancer[J]. *Nature*, 2014, 510(7505): 407–411.

[34] Hientz K, Mohr A, Bhakta-Guha D, et al. The role of p53 in cancer drug resistance and targeted chemotherapy[J]. *Oncotarget*, 2017, 8(5): 8921–8946.

[35] Zuber J, Shi J, Wang E, et al. RNAi screen identifies Brd4 as a therapeutic target in acute myeloid leukaemia[J]. *Nature*, 2011, 478(7370): 524–528.

[36] Inkol JM, Hocker SE, Mutsaers AJ. Combination therapy with cannabidiol and chemotherapeutics in canine urothelial carcinoma cells[J]. *PLoS One*, 2021, 16(8): e0255591.